




Article

Recovery of Copper and Magnetite from Copper Slag Using Concentrated Solar Power (CSP)

Daniel Fernández-González ^{1,*} , Janusz Prazuch ² , Íñigo Ruiz-Bustanza ³ , Carmen González-Gasca ⁴, Cristian Gómez-Rodríguez ⁵ and Luis Felipe Verdeja ⁶

¹ Nanomaterials and Nanotechnology Research Center (CINN-CSIC), Universidad de Oviedo (UO), Principado de Asturias (PA), Avda. de la Vega, 4-6, 33940 El Entrego, Spain

² Department of Physical Chemistry and Modelling, Faculty of Materials Science and Ceramics, AGH University of Science and Technology, 30-059 Krakow, Poland; prazuch@agh.edu.pl

³ Departamento de Ingeniería Geológica y Minera, Escuela Técnica Superior de Ingenieros de Minas y Energía, Universidad Politécnica de Madrid, 28003 Madrid, Spain; inigo.rbustanza@upm.es

⁴ Vice-Rector's Office, Universidad Internacional de Valencia, 46002 Valencia, Spain; cgonzalezg@universidadviu.com

⁵ Departamento de Mecánica, Facultad de Ingeniería, Campus Coatzacoalcos, Universidad Veracruzana, Av. Universidad km 7.5 Col. Santa Isabel, Coatzacoalcos 6535, Veracruz, Mexico; crisgomez@uv.mx

⁶ Department of Materials Science and Metallurgical Engineering, Oviedo School of Mines, Energy and Materials, University of Oviedo, 33004 Oviedo/Uviéu, Spain; lfv@uniovi.es

* Correspondence: d.fernandez@cinn.es



Citation: Fernández-González, D.; Prazuch, J.; Ruiz-Bustanza, Í.; González-Gasca, C.; Gómez-Rodríguez, C.; Verdeja, L.F. Recovery of Copper and Magnetite from Copper Slag Using Concentrated Solar Power (CSP). *Metals* **2021**, *11*, 1032. <https://doi.org/10.3390/met11071032>

Academic Editor: Fernando Castro

Received: 31 May 2021

Accepted: 24 June 2021

Published: 27 June 2021

Publisher's Note: MDPI stays neutral with regard to jurisdictional claims in published maps and institutional affiliations.



Copyright: © 2021 by the authors. Licensee MDPI, Basel, Switzerland. This article is an open access article distributed under the terms and conditions of the Creative Commons Attribution (CC BY) license (<https://creativecommons.org/licenses/by/4.0/>).

Abstract: On the one hand, copper slag is nowadays a waste in copper pyrometallurgy despite the significant quantities of iron (>40 wt. %) and copper (1 to 2 wt. %). On the other hand, solar energy, when properly concentrated, offers great potential in high-temperature processes. Therefore, concentrated solar power (CSP) could be used in the treatment of copper slag to transform fayalite into magnetite and copper sulfides and oxides into copper nodules. This is the objective of this paper. The results show that fayalite was partially decomposed into magnetite and silica. Moreover, copper nodules (65–85 wt. % Cu) were identified in the treated samples, while the initial slag, analyzed by X-ray diffraction, X-ray fluorescence, and SEM-EDX, did not show the presence of metallic copper. Finally, the treated copper slag was crushed and grinded down to 40 μm , and two fractions were obtained by magnetic separation. The magnetic fraction (85%) was mainly comprised of magnetite, while the non-magnetic fraction (15%) had 5–10 wt. % Cu. Considering the experimental results, 7.5–18 kg Cu/t slag might be recovered from the slag. A preliminary economic analysis, considering the current copper price, indicates that only the recovery of copper could represent a significant economic benefit (>30 €/t slag). Therefore, CSP might be a potential candidate for the treatment of copper slag to recover copper and iron.

Keywords: concentrated solar power (CSP); copper slag; copper; environment; sustainable metallurgy; solar energy

1. Introduction

Copper is one of the most mined metals on the Earth due to the applications of this metal in different fields. However, a lot of tailing material, currently unprocessed, is generated in the process, and provides a huge opportunity to use concentrated solar power (CSP).

The pyrometallurgical technique is the most important to produce copper, and the smelting conversion process is the most widely used within this route [1]. Thus, 80% of the copper is currently produced by the concentration, smelting, and refining of sulfide ores [2], which include chalcopyrite (CuFeS_2), bornite (Cu_5FeS_4), and chalcocite (Cu_2S). Different products are generated in the fusion conversion process (Figure 1). These include matte, which is heavy and contains most of the copper as sulfide (it is later treated in the

converter to obtain blister copper, and finally metallic copper is produced after fire refining and electrowinning) and slag, which contains most of the iron as fayalite.

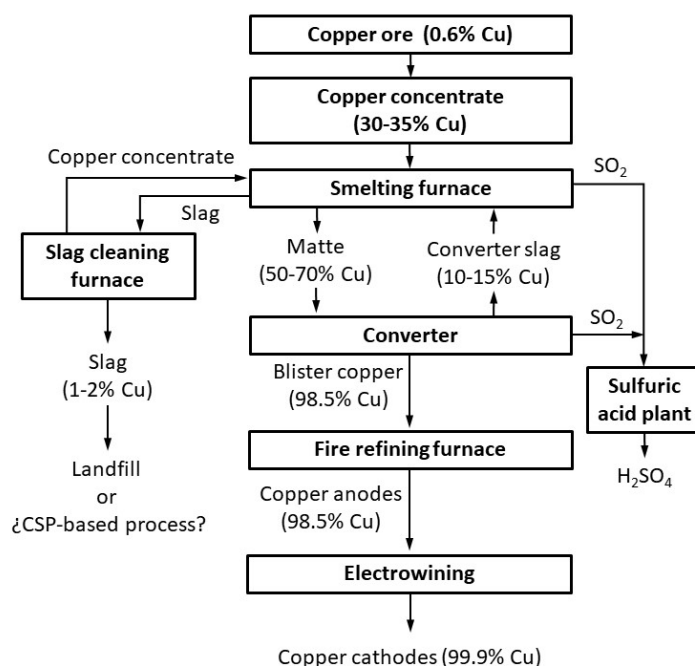


Figure 1. Flow diagram of the smelting conversion process of copper.

Two slags are produced in the smelting conversion process: first, in the smelting furnace, and second in the converter. However, these slags contain (apart from fayalite and magnetite, which are the main phases) significant quantities of copper (sulfide (matte) dragged or trapped by the slag, or oxide associated with other oxides of the slag [1,3]). The slags are reprocessed in the smelting furnace or in the slag cleaning furnace (electric furnaces, where carbon and pyrite are used as additives) to recover some of the copper. Finally, the final slag is disposed of in a controlled landfill when the copper concentration is approximately in the range 1 to 2 wt. % Cu.

Copper slags might be considered a residue/by-product with great potential due to both the copper (1–2 wt. % Cu) and iron (>40 wt. % [4–10]) contents as a secondary resource for metal recovery [11]. A total of 20 Mt of primary copper are produced worldwide, and this involves 45 Mt of slag generated in the process (2.2–3 tons of slag/ton copper [2,12,13]), which would represent >20 Mt Fe and 0.5–1 Mt Cu yearly sent to controlled landfills. Therefore, copper slag represents an environmental impact [4]: risks of heavy metals lixiviation, a visual impact, and sometimes occupation of cultivable areas. Researchers have tried to find a use for copper slags, but a massive industrial utilization has still not been found [14]. Copper slags have been used as abrasives (polishing and cleaning) for metallic structures [15,16] and mainly in the building industry: concrete manufactured with copper slag [5]; copper slags as fine particles in concrete manufacturing [13]; copper slag as a replacement for the sand in cements [9]; copper slag as a filler in glass–epoxy composites [17]; and copper slag as a construction material in bituminous pavements [18]. Research has also focused on the recovery of iron from the slag: by using coke as reductant of the copper oxide and the magnetite [19]; by modifying the molten slag with the purpose of promoting the mineralization of recoverable mineral phases and inducing the growth of the mineral phases [20]; by using a method based on coal, Direct Reduction Iron (DRI), and magnetic separation [21]; by means of a process based on aluminothermic reduction [22]; by reduction in an electric furnace with the objective of obtaining a Cu–Pb–Fe alloy [23]; by carbothermic reduction to transform the copper slag into pig iron and glassy material [24];

by irradiation with a microwave as a support of the carbothermal method [25]; or by reduction with coke powders and magnetic separation [26].

Solar energy has been widely used in materials science and metallurgy [27]. The main types of research in the field of metallurgy carried out with concentrated solar power (CSP) are listed in Table 1.

Table 1. Main types of research in the field of metallurgy and mineral processing using CSP (abbreviations: OSF, Odeillo Solar Furnace; PSI, Paul Scherrer Institute; WIS, Weizmann Institute of Science; UKR, Institute for Problems of Materials Science of NAS of Ukraine; PSA, Plataforma Solar de Almería).

Material	Process	Temperature	Installation	Researcher
Si	Dissociation of Si ₃ N ₄ by carbothermal reduction of SiO ₂ under an N ₂ atmosphere	>1400 °C	OSF	Jean P. Murray, Gilles Flamant, Carolyn J. Roos [28]
Si	Carbothermic reduction of SiO ₂ under vacuum conditions at a high temperature	1725–2000 °C	PSI	Peter G. Loutzenhiser, Ozan Tuerk, Aldo Steinfeld [29]
Al	Production of aluminum via carbothermal reduction	>2000 °C	PSI and OSF	Jean P. Murray [30–32]
Al	Production of aluminum using both electricity and heat generated using solar energy	≈1000 °C	UKR	Y. M. Lytvynenko [33]
Zn	Production of zinc via CSP to be used in water and carbon dioxide splitting (scaled up to demonstration plant scale [34])	>1750 °C	Mainly at the PSI, OSF, and WIS	E. A. Fletcher, R. D. Palumbo, T. Osinga, M. Epstein A. Steinfeld, C. Wieckert, L. Schunck, W. Villasmil, E. Koepft, and others [35–45]
Fe, Mn, Cd	Treatment of different materials containing iron	>1100 °C	Mainly at the PSI, PSA, OSF, and WIS	F. Sibieude, A. Steinfeld, E. A. Fletcher, I. Ruiz-Bustinza, J. Mochón and others [46–49]

Concentrated solar power (CSP) has also been used in materials processing and non-metallic materials. The use of CSP in these latter fields can be found in Fernández-González et al. [27]. The application of CSP in materials science and metallurgy has been widely investigated by our research group. The following fields can be mentioned: synthesis of calcium aluminates [50], iron metallurgy [46,51,52], the treatment of Basic Oxygen Furnace (BOF) slag [53], the production of silicomanganese [54], and transformations in the Ca-Si-O system [55].

The utilization of concentrated solar power (CSP) to treat copper slag is proposed in this paper. Since most of the copper is produced in mines located in the west of the American continent (from Arizona (United States) to Chile), where high values of solar radiation are measured, the use of CSP might have great potential to recover copper and iron from slags. Figure 2 shows a flow-sheet of the process to examine Cu tailings using CSP. The main results are schematically indicated. Therefore, the aims of the research are: to transform the fayalite into magnetite, as iron could be collected from the slag as magnetite using magnetic methods; and to transform copper oxide and copper matte (the occluded matte in the slag) into metallic copper and concentrate it.

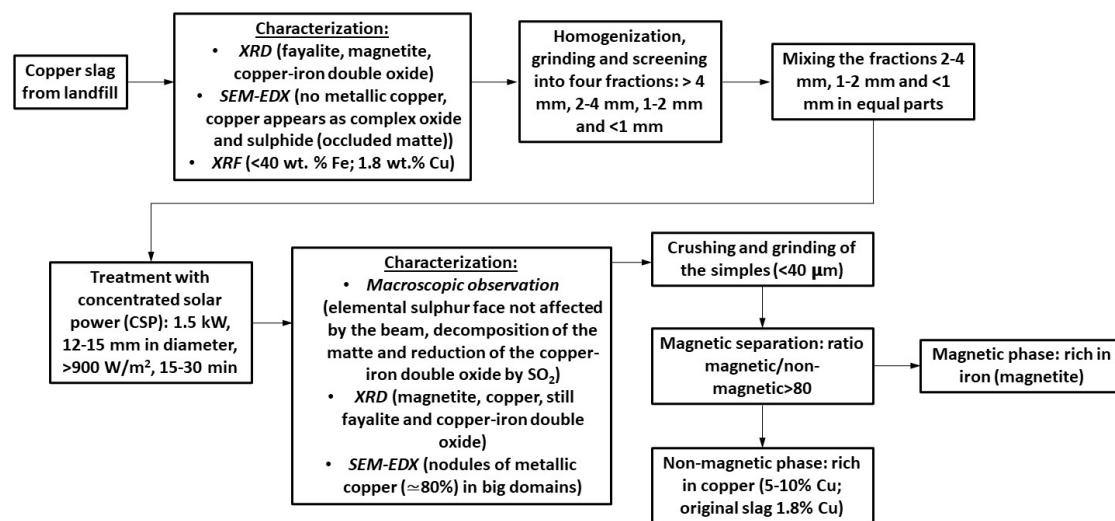


Figure 2. Flow-sheet for the process to examine Cu tailings using CSP.

2. Materials and Methods

2.1. Materials

Original copper slag from the slag cleaning furnace was used in the experiments (Figure 1). It was homogenized, milled, and screened into four granulometric fractions: >4 mm, 2–4 mm, 1–2 mm, and <1 mm, and only the last three were considered to facilitate chemical reactions. They were mixed in equal parts (33.3%).

The chemical composition of the slag (Table 2) was obtained by X-ray fluorescence. X-ray fluorescence measurements were performed with a wavelength dispersive X-ray fluorescence spectrometer (Axios, PANalytical) equipped with a Rh-anode X-ray tube with a maximum power of 4 kW. All samples were measured in a vacuum with a 15–50 eV energy resolution. For quantitative analysis of the spectra, the PANalytical standardless analysis package Omnian was used.

Table 2. Elemental analysis of the copper slag (wt. %) determined by X-ray fluorescence.

Fe	O	Si	Al	Cu	Ca	Na	S	Others
42.82	36.15	10.36	3.24	1.84	1.76	0.99	0.52	2.32

Original copper slag was studied by X-ray diffraction of powders. X-ray diffraction measurements were conducted with an Empyrean PANalytical diffractometer using $\kappa\alpha_1$ and $\kappa\alpha_2$ radiation from a Cu anode. All measurements were performed with the Bragg–Brentano setup at room temperature with a 0.006° step size in the $5\text{--}90^\circ$ 2θ scanning range and 145 s of measurement time for each step. Data analysis and the peak profile fitting were carried out using X Powder 01.02 (Database PDF2 (70 to 0.94)). The quantitative analysis of the crystalline phases was also performed using the software X Powder12 Ver. 01.02.

The main crystalline phase in the slag was fayalite (Fe_2SiO_4), $85.80 \pm 1.30\%$ in the quantitative analysis. Other important crystalline phases were magnetite (Fe_3O_4) and copper–iron oxide (cuprospinel, CuFe_2O_4 , with Cu^{2+} and Fe^{3+}), $7.90 \pm 1.60\%$ and $6.20 \pm 1.80\%$, respectively, in the quantitative analysis.

2.2. Experimental Procedure

Tests were performed in a vertical axis 1.5 kW solar furnace located in Font Romeu-Odeillo-Via (PROMES-CNRS laboratory (Procédés, Matériaux et Énergie Solaire—Centre National de la Recherche Scientifique), Font Romeu-Odeillo-Via, France). The operation of the solar furnace is based on making solar radiation converge on a small surface (12–15 mm

in diameter), called the focal point, using optical systems (or mirrors). In the case of this furnace (Figure 3), a heliostat directs sun radiation towards a parabolic concentrator (2.0 m in diameter), which makes radiation converge at the focal point, where the experimental device is located.

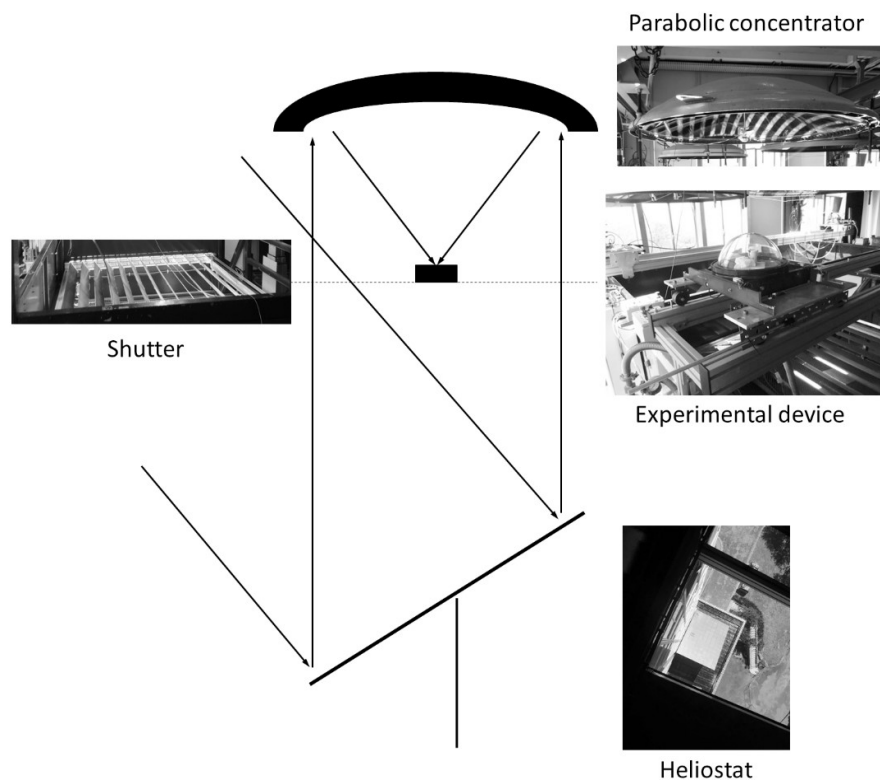


Figure 3. Scheme of the equipment used in the experiments.

This solar furnace allows for a maximum concentration of 15,000 times the incident radiation. It is possible to control the value of the power applied to the sample by a shutter (Figure 3). This way, the value of the power can be calculated with Equation (1).

$$\text{Power (W)} = \text{Incident radiation (W/m}^2\text{)} \times 1.5 \times \text{ShOp}/100, \quad (1)$$

where ShOp is the shutter opening value, which is 0 when the shutter is completely closed and 100 when it is totally open. Fast heating and cooling rates are usual in solar furnaces. This allows us to obtain metastable phases even at room temperature. The temperature was controlled by a type K thermocouple (chromel-alumel thermocouple). It was located at half height outside of the crucible. The maximum temperature inside of the crucible (in the range 1700–1900 °C, calculated by Finite Element Method (FEM)-based software) is reached when the temperature stabilizes at approximately 600 ± 30 °C in this thermocouple. The sample was held at the maximum temperature for 10 min. Both the temperature and time were enough to perform the experiments according to the thermodynamic calculations (theoretical) and, thus, achieve the decomposition of the fayalite into magnetite and silica, and the formation of metallic copper nodules from copper oxide (and from the occluded matte) [56]. From the thermodynamics point of view, the decomposition of the fayalite is possible in an oxidizing environment, while obtaining metallic copper is favorable under reductant conditions [56]. Both processes compete between them and it is not possible to complete them in a single step. Reductant agents were not used during the experiments. However, the addition of reductant agents would favor the obtaining of metallic copper. In this case, the decomposition of the fayalite into magnetite and silica would be less favorable. Future research might focus on the addition of wastes from other metallurgies to promote

the formation of copper nodules or fayalite decomposition. An option is the utilization of blast furnace powders. This by-product is rich in carbon, which would promote reductant conditions, and rich in iron, which would increase the iron content in the slag.

Crucibles of tabular alumina (55 mm in height, 30 mm in upper diameter, 25 mm in lower diameter, and 3 mm in thickness) were used in the experiments. Samples were located under a glass chamber as in Figure 3. No special atmosphere was used in the experiments. However, the glass chamber was connected to a pump to facilitate the extraction of the gases generated in the process. This ensured a pressure of 0.85 atm inside the chamber.

Seven experiments were carried out in total. The conditions are collected in Table 3. The duration of the experiments was controlled by the temperature in the thermocouple T1. Samples were held at the maximum temperature for 10 min once this temperature had been reached. Except for the samples CuSin3 and Cusinbonus, the rest of the samples were subjected to similar values of power.

Table 3. Conditions used in the experiments.

Sample	Lime	Shutter Opening	Time (min)	Average Incident Radiation (W/m ²)	Power (W)
CuSin1	No	80	20	941.2	1129
CuSin2	No	88	25	955.8	1262
CuSin3	No	41	30	915.5	563
Cusinbonus	No	60	23	867.8	781
CuCon1 (stop in the middle of the experiment)	Yes	92	-	938	1294
CuCon2	Yes	100	15	939.5	1409
CuCon3	Yes	84	20	973	1226

3. Results

3.1. Macroscopic Analysis

Samples were subjected to visual observation. Some remarkable questions can be deduced from this analysis. The average dimensions of the volume affected by the beam of CSP were: 19 mm in diameter and 13 mm in depth. This layer of treated material (material that completely melted during the process) blocks the heating until melting of all the material available in the crucible. Therefore, the slag remains unreacted below the above-indicated layer. On another note, the sample was clearly magnetic after the treatment with CSP. The initial slag was not magnetic (fayalite was the main constituent of the initial slag, which is not magnetic), so the magnetite content increased during the process and became the main constituent of the final product.

On another note, elemental sulfur (greenish yellow) is identified in the face located in contact with the unaffected material. It is the product of the thermal decomposition of the occluded matte (copper sulfides). In this context, Winkel studied the thermal decomposition of copper sulfides under concentrated irradiation [57]. He observed that metallic copper, iron sulfide, and elemental sulfur can be obtained after the treatment of copper concentrates at a high temperature under an inert atmosphere. To a certain extent, copper slag always contains a certain amount of copper sulfides as occluded matte (a binary mixture of Cu₂S and FeS). The elemental analysis of the slag used in our experiments indicates 0.52 wt. % S, which is combined with iron and copper. Moreover, our experiments were performed under an ambient atmosphere impoverished in oxygen promoted by the utilization of the glass chamber and the pump. Additionally, the layer of molten slag blocks the circulation of gases (oxygen) through the slag and there is both a high temperature and an inert atmosphere in part of the charge. Under these conditions, occluded matte can decompose and give copper, as in Winkel's work [57]. This explains the presence of metallic copper in the final samples (apart from the decomposition of the copper oxides under reductant

conditions). It is necessary to consider that this mechanism is very limited due to the small proportion of occluded matte (there was around 0.52 wt. % S in the initial sample).

3.2. SEM-EDX

Samples were also analyzed using a scanning electron microscope and point analysis. The objective of this analysis was to check for both the presence of copper and the increase in magnetite in the final samples that resulted from the treatment with solar energy. Copper nodules were identified using this technique (65–85 wt. % Cu). Magnetite was also identified, the same as fayalite. Four representative SEM-EDX analyses of the treated samples are shown in Figure 4.

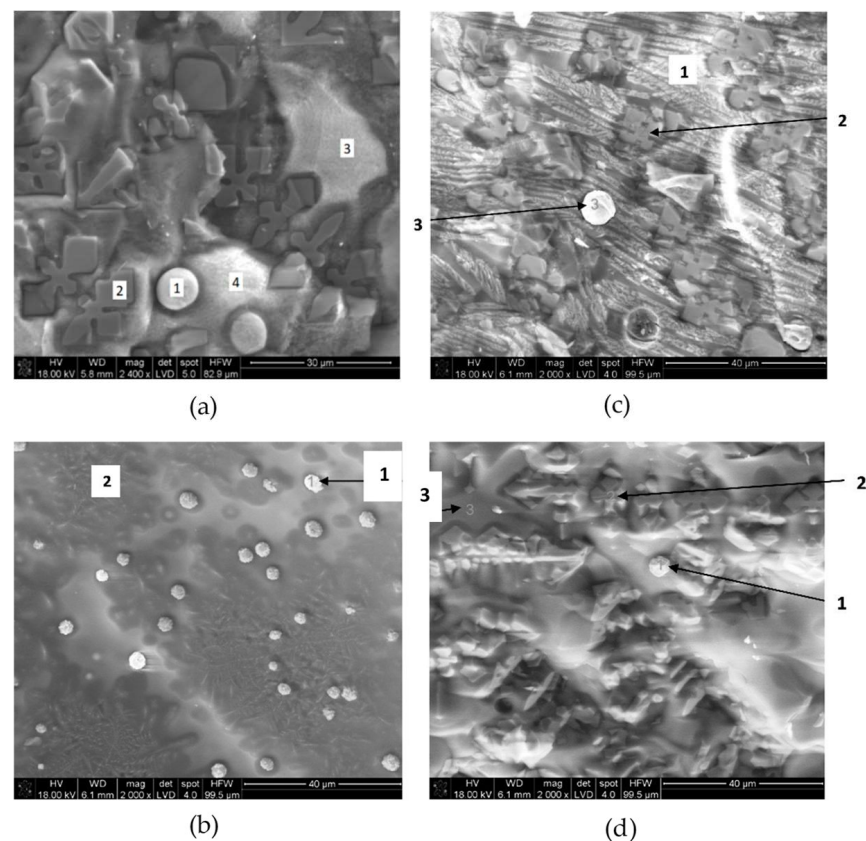


Figure 4. (a) SEM-EDX sample identified as CusinBonus; (b) SEM-EDX sample identified as CuCon3; (c) SEM-EDX sample identified as CuCon1; (d) SEM-EDX sample identified as CuSin1.

A representative zone of the sample CusinBonus is observed in Figure 4a. Point 1 corresponds to a copper-rich nodule (79.12 wt. % Cu; 9.66 wt. % Fe; 5.02 wt. % O); point 2 shows magnetite; while point 3 and point 4 represent non-decomposed fayalite. It was observed that the presence of copper-rich nodules causes the impoverishment in copper of the surrounding areas.

A representative zone of the sample CuCon3 can be observed in Figure 4b. Point 1 corresponds to copper-rich nodules (79.03 wt. % Cu; 7.63 wt. % Fe; 5.72 wt. % O; 0.33 wt. % S) and point 2 indicates a ferrite of calcium and silicon. In the case of the sample CuCon1 (Figure 4c), it is possible to check that point 1 corresponds to the fayalite, point 2 represents the magnetite, while point 3 represents the copper-enriched nodule (80.51 wt. % Cu; 10.01 wt. % Fe; 3.71 wt. % O).

Sample CuSin1 (Figure 4d) was also analyzed using SEM-EDX. Point 1 represents copper nodules (82.45 wt. % Cu; 8.98 wt. % Fe; 2.91 wt. % O), point 2 represents magnetite, while point 3 represents non-decomposed fayalite.

The formation of magnetite is also significant in the experiments due to the decomposition of the fayalite (into magnetite and silica). Therefore, oxidizing conditions were also verified during the experiments because magnetite was clearly formed. Figure 5 shows a large region of the sample where magnetite was massively formed. Points 1, 2, 3, and 5 (40–50 wt. % Fe, 25–29 wt. % O) represent iron oxides. The well-developed tetrahedrons of magnetite in the region represented by point 3 can clearly be observed. Magnetite refers in this manuscript to a series of phases belonging to the iron spinel as magnesioferrite (MgFe_2O_4), magnetite (FeFe_2O_4 , where one Fe is +2 and two Fe's are +3, respectively), and maghemite ($\gamma\text{-Fe}_2\text{O}_3$, Fe (II)-deficient magnetite). Cuprospinel (CuFe_2O_4) would also belong to this series of iron spinel. Point 4 corresponds to the non-decomposed fayalite (22.72 wt. % Si, 36.52 wt. % O, 11.58 wt. % Si).

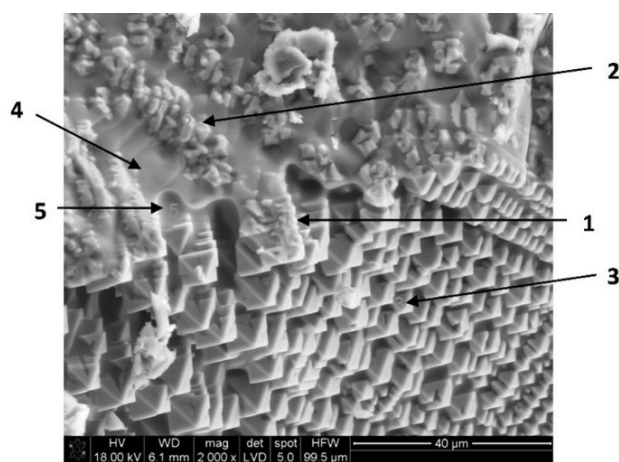


Figure 5. SEM-EDX sample identified as CuCon2.

3.3. Size of the Nodules

Strictly, copper nodules are not formed. It would be more convenient to talk about nodules enriched in copper (65–85 wt. % Cu; 5–10 wt. % Fe; 2–10 wt. % O; <3 wt. % S). The size of the nodules was determined using the scanning electron microscope in different sections and SEM images obtained from crushed final specimens. Most of the nodules had a size between 5 and 10 μm (see Figure 6). However, individual copper nodules with a larger size were detected in some samples (between 20 and 35 μm). The size of the nodules will define the grinding size for the subsequent separation. Figures 7–9 show fields of copper nodules formed during the treatment of the copper slag with CSP. It is possible to see that reductant conditions were also promoted during the experiments since copper nodules are formed. The presence of magnetite formed during the decomposition of the fayalite promotes an environment with reductant potential; this ensures the formation of the copper nodules and prevents during the cooling the reversion of the process. It is also necessary to consider that some of the copper nodules are formed because of the occluded matte decomposition according to the mechanism proposed by Winkel [57]. The clustering mechanism is evident (Figures 7–9) because many copper nodules are formed in the same field. However, the growth mechanism did not take place because these nodules did not merge to form larger nodules. This is a consequence of the short duration of the treatment, the viscosity of the liquid phase (due to the presence of magnetite), and the high cooling rate.

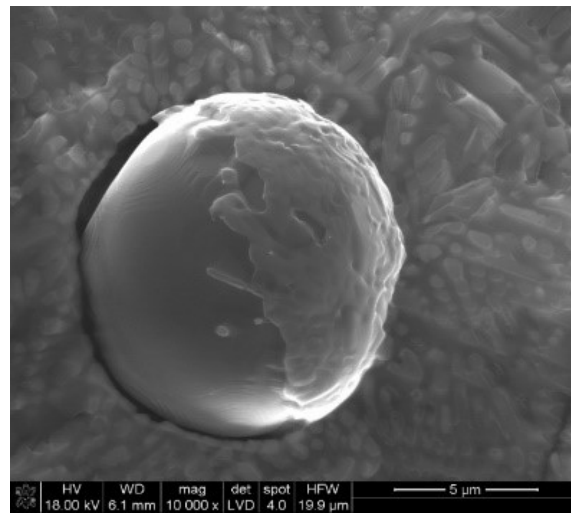


Figure 6. SEM-EDX image of a copper nodule.

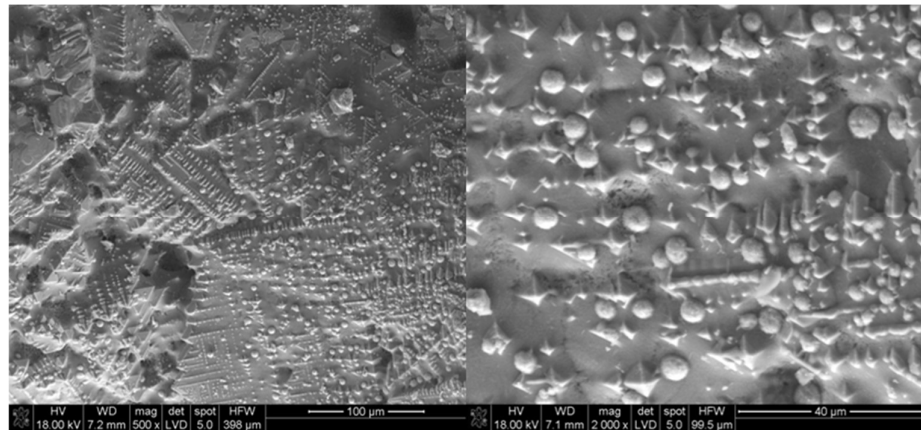


Figure 7. SEM-EDX sample identified as CuCon1.

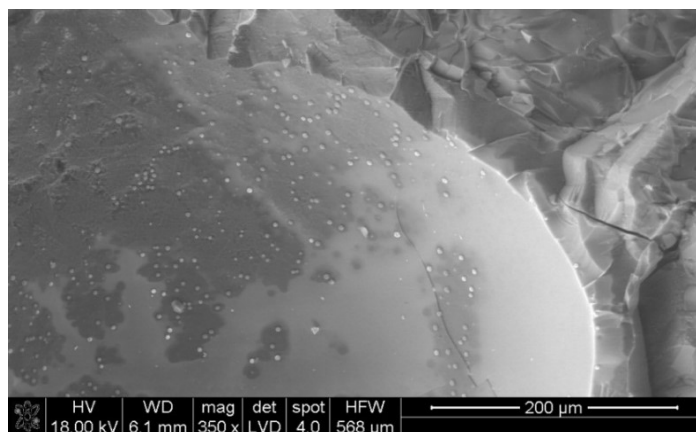


Figure 8. SEM-EDX sample identified as CuCon3.

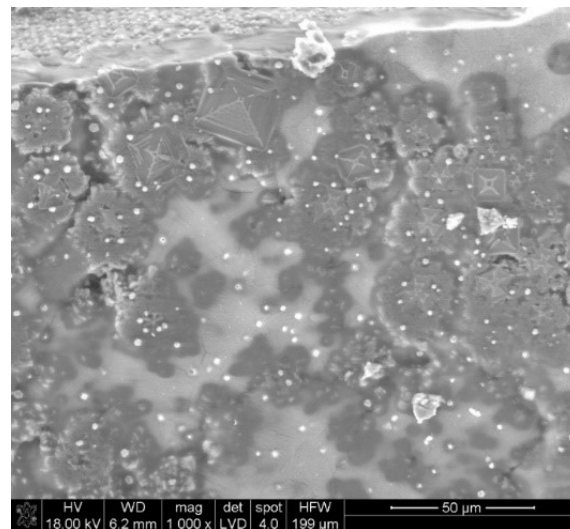


Figure 9. SEM-EDX sample identified as CuSin3.

3.4. Grinding and Magnetic Separation

Treated samples (19 mm in diameter and 13 mm in thickness) were crushed and grinded down to 40 μm . Then, they were separated into two fractions: magnetic and non-magnetic. Each fraction was analyzed by X-ray diffraction and X-ray fluorescence. In some cases, the quantity of sample was not sufficient to separate magnetic and non-magnetic phases, so analyses were made on the available fraction. In those samples where both magnetic and non-magnetic fractions were available, the ratio magnetic to non-magnetic was >80 (average value: 83.3625, in weight). This is reasonable because it was expected that the treated material would be magnetic due to the partial transformation of the fayalite into magnetite under the conditions of the experiments.

The X-ray fluorescence results are collected in Tables 4 and 5. The copper concentrated in the non-magnetic phase 3–6.5 times with respect to the initial slag (1.84 wt. % Cu). The grade in mining is an important factor about how much a deposit is worth. The average grade of copper ores in the 21st century is below 0.6% Cu. This means that copper slags might be a potential secondary source of copper, especially if it is possible to concentrate copper using free and renewable energy sources (as concentrated solar power (CSP)).

Table 4. X-ray fluorescence results.

Element	Original Copper Slag	CuSin1 Magnetic	CuSin2		CuSin3	
			Magnetic	Non-Magnetic	Magnetic	Non-Magnetic
Cu	1.84	1.34	1.29	11.72	1.27	7.09
Fe	42.82	38.53	44.75	43.51	45.45	45.34
O	36.15	37.98	36.17	32.50	35.94	33.43
Si	10.36	12.28	10.39	6.20	9.85	6.90
Al	3.24	5.94	2.47	1.16	2.67	1.82
Ca	1.76	0.88	1.06	1.64	1.10	2.08
Na	0.99	0.71	0.87	0.30	0.78	0.43
K	0.69	0.64	0.75	0.56	0.76	0.62
S	0.52	0.25	0.63	0.88	0.60	0.58
Others	1.63	1.46	1.62	1.52	1.58	1.70

Table 5. X-ray fluorescence results.

Element	Cubonus Magnetic	CuCon1		CuCon2		CuCon3 Magnetic
		Magnetic	Non-Magnetic	Magnetic	Non-Magnetic	
Cu	0.88	1.28	7.25	1.01	5.34	1.52
Fe	39.05	42.21	23.24	38.02	32.27	38.26
O	37.63	34.64	35.68	37.83	34.78	37.55
Si	11.63	7.22	6.42	11.48	7.32	11.31
Al	5.80	2.85	10.02	6.50	5.24	6.31
Ca	1.93	8.52	14.29	2.05	12.24	2.22
Na	0.62	0.47	0.27	0.69	0.33	0.53
K	0.67	0.62	0.46	0.67	0.46	0.65
S	0.25	0.71	0.76	0.30	0.58	0.24
Others	1.53	1.47	1.61	1.45	1.44	1.42

Powdered samples were analyzed using the X-ray diffraction technique in homogenized samples. The objective was to evaluate the phases that resulted from the treatment of copper slag with concentrated solar power (CSP). Figures 10–13 compare the original slag with the treated slag (not separated), the treated slag (magnetic phase), and the treated slag (not magnetic). The quantity of non-magnetic fraction was very limited, so diffraction analyses are available for only a few samples. If the peaks are analyzed, it is possible to check that the main crystalline phase in the original slag was the fayalite (Fe_2SiO_4), being the magnetite (Fe_3O_4) and cuprospinel (CuFe_2O_4) the other important crystalline phases. It can be observed that the peaks of the fayalite decrease in intensity for the treated samples because the quantity of magnetite increases, being particularly relevant in the case of the magnetic sample. The non-magnetic phase mainly comprises fayalite and copper, which is consistent with the SEM analyses. Copper sulfides (Cu_2S , $\text{Cu}_{0.98}\text{S}$) and copper oxide (CuO) were also identified, which indicates that not all the copper in the initial slag decomposed during the treatment and that the nodules are not from pure copper. The presence of magnetite formed during the treatment provides an environment with reductant potential and prevents the oxidation of the copper to a certain extent.

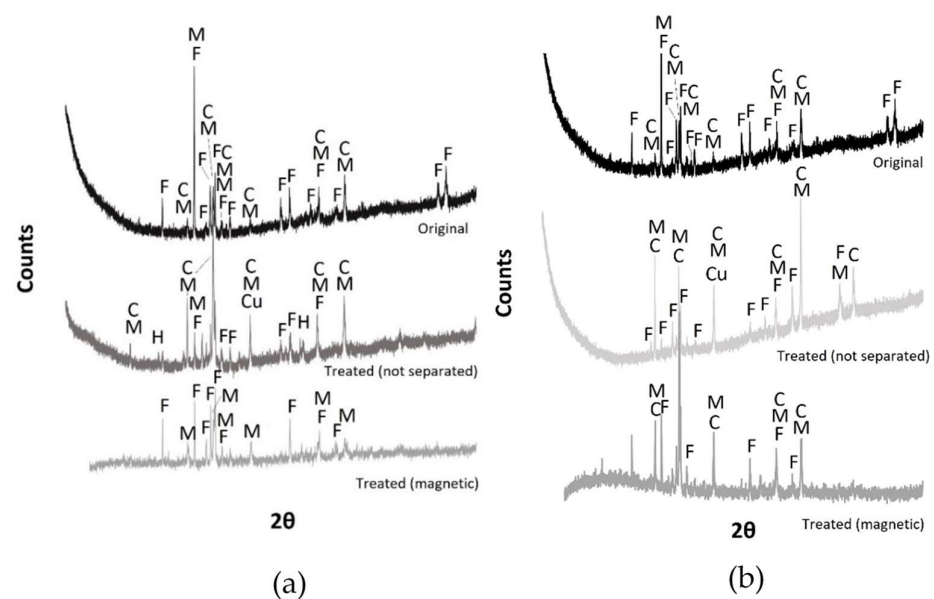


Figure 10. (a) Specimen Cubonus (C, CuFe_2O_4 ; F, Fe_2SiO_4 ; M, Fe_3O_4 and all the iron spinel; Cu, metallic copper). (b) Specimen CuSin1 (C, CuFe_2O_4 ; F, Fe_2SiO_4 ; M, Fe_3O_4 and all the iron spinel; Cu, metallic copper).

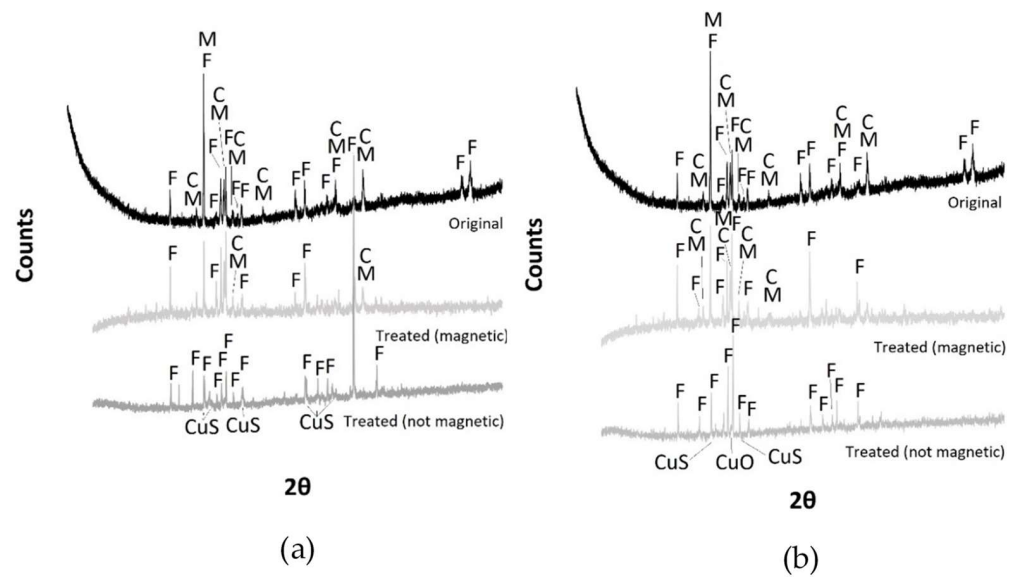


Figure 11. (a) Specimen CuSin2 (C, CuFe₂O₄; F, Fe₂SiO₄; M, Fe₃O₄ and all the iron spinel; CuS, Cu₂S, Cu_{0.98}S). (b) Specimen CuSin3 (C, CuFe₂O₄; F, Fe₂SiO₄; M, Fe₃O₄ and all the iron spinel; CuS, Cu₂S, Cu_{0.98}S; CuO).

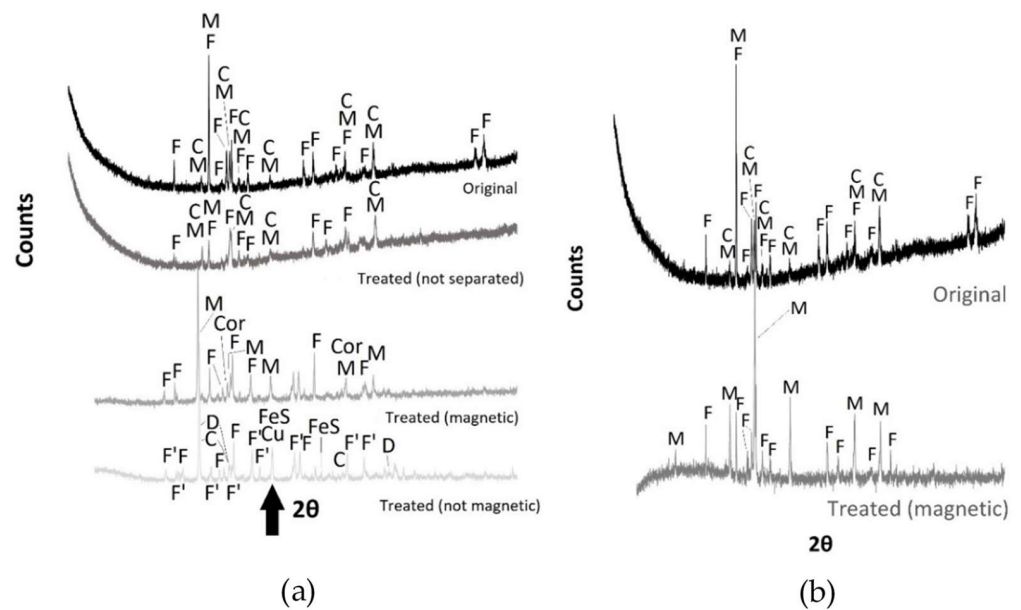


Figure 12. (a) Specimen CuCon1 (C, CuFe₂O₄; F, Fe₂SiO₄; M, Fe₃O₄ and all the iron spinel; Cu, metallic copper; F', Fe_{0.92}Mg_{1.08}O₄S; D, CaMg(SiO₃)₂; FeS). (b) Specimen CuCon3 (C, CuFe₂O₄; F, Fe₂SiO₄; M, Fe₃O₄ and all the iron spinel).

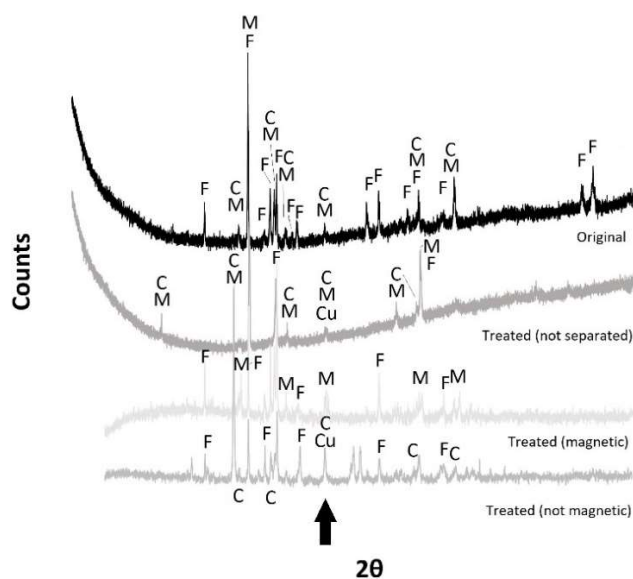


Figure 13. Specimen CuCon2 (C, CuFe_2O_4 ; F, Fe_2SiO_4 ; M, Fe_3O_4 and all the iron spinel; Cu, metallic copper).

4. Discussion

In 1944, Ellingham studied the representation and quantitative evaluation of the periodic system elements' different affinities (80% of the elements of the periodic system are metallic) by the O_2 (g) and S_2 (g) through the standard free energy of the reactions [58,59]. As a result of his investigations, Ellingham's diagrams were published (these diagrams were enriched/complemented by Richardson and Jeffers in 1948) [60].

Thermodynamically speaking, the standard free energy of the reactions of the metallic oxides' /sulfides' formation is related to the equilibrium constant. In this way, it is possible to make a classification of the oxides and sulfides into three categories: oxides and sulfides that are easily reduced, oxides and sulfides situated in an intermediate position, and oxides and sulfides that are difficult to reduce.

However, for some oxides and sulfides that are easily reduced, such as the combinations of copper with either sulfur or oxygen, it is possible that the thermodynamic stability is changed for these compounds with the simple action of the temperature, and the stable phase would be the metal and neither the oxide nor the sulfide. The temperature at which the thermodynamically stable phase is the metal (neither the oxide nor the sulfide) is known as inversion temperature. Another situation that can take place is that in those elements with different oxidation states, the oxide stable at a low temperature is different from the stable oxide at a higher temperature (the transformation of magnetite (Fe_3O_4) into hematite (Fe_2O_3) at a high temperature takes place at around 1400 °C). In this context, fayalite decomposition into magnetite and silica takes place under an ambient atmosphere with oxidizing potential. As the oxygen available in the experiments is very limited due to the utilization of the glass chamber and the pump to remove the gases, the complete decomposition of the fayalite and the oxidation of the magnetite to obtain hematite are not possible. This is the reason for having such a quantity of magnetite at the end of the process (a similar situation was observed when treating BOF slags from the steel industry [53]), which otherwise is advantageous since it might be easily separated using magnetic methods.

In the case presented in this paper, either the Cu_2S or the Cu_2O , in slightly reductant environments propitiated by the presence of Fe_3O_4 (magnetite) and FeO (wustite), cause the thermodynamically stable species for the copper to be the metallic copper and not the oxide or the sulfide [56].

In this way, it is feasible that, when treating a copper slag (which mainly comprises fayalite) that contains in the form of solid solution or as sulfides or oxides dispersed in a

matrix of fayalite copper atoms in quantities of around 2 wt. %, the reduction of copper in an environment controlled by the oxidizing potential of the FeO–Fe₃O₄ system takes place (the same could be indicated with respect to the fact that the reductant for the fayalite would be the FeO). The high heating rate, but also the high cooling rate, that can be reached in solar furnaces propitiate that the phases obtained at high temperatures could be also observed at room temperature due to the kinetics, and, in this way, remarkably, changes are not produced (it possible to think about the Time–Transformation–Temperature curves) [61,62]. However, the short duration of the treatments impedes the development of the copper nodules.

The recovery of both iron and copper from copper slags has been studied using concentrated solar power (CSP), but in a preliminary manner. This research offers results about the utilization of CSP to transform fayalite into magnetite, and to decompose CuFe₂O₄ to recover copper from the slag (and additionally to transform occluded copper matte into copper). Once the feasibility of using solar energy in this field has been demonstrated, it will be time to think about the improvement of the experimental conditions for the purpose of maximizing the transformation of fayalite into magnetite, and the destruction of both the CuFe₂O₄ and the occluded matte. This way, it is reasonable to think about the design of the reactor, and even evaluating the possibility of scaling up the process to the industrial scale. The commercialization of the process will depend on how much copper can be recovered using this process, but also will depend on how much iron can be collected as magnetite. A problem could arise from the installation costs for this technology as they are in the range of other high-energy technologies, such as plasma or even lasers [63], and because it is still an immature technology (in the field of materials). In fact, concentrated solar power (CSP) has not been scaled up to the industrial level for materials science or metallurgical applications [27]. Apart from the technical limitations (such as the obtaining of high-quality mirrors at a reasonable price), the above-mentioned economical limitations should be considered. It is necessary to consider that nowadays copper slags are disposed of in a controlled landfill despite the copper and iron contents. If it was possible to recover both elements, the cost of obtaining both elements (transportation costs, installation costs, etc.) should be lower than the revenues produced by selling the copper and iron concentrates. Additionally, copper, as observed in the analysis, is not pure copper, and for that reason it should be treated after the process. Further studies should be performed to increase the purity of the copper (and to make the copper nodules grow up to a reasonable size for the subsequent metallurgical operations), but also to study the question of how to separate all phases in a proper way. Anyway, it is possible to concentrate 3–6.5 times the copper in the non-magnetic phase. If the commercial copper grade for copper oxides is considered (0.6 wt. %), the copper concentrate obtained using solar energy would be 3–6.5 times richer than the commercial one using a waste that is not necessary to mine. Another potential application of concentrated solar power (CSP), also in copper metallurgy, is in the furnaces used to treat slags before their disposal, where significant electrical energy is used to heat the furnaces, although the CSP-based process is still not competitive nowadays.

A preliminary study of the potential economic impact of the treatment of the slag with CSP was carried out. The slag, as was checked in the characterization, mainly comprises fayalite (>85%). For that reason, energy requirements were calculated considering only this phase. A total of 275 kWh/t slag is the latent heat, and 125 kWh/t slag is the enthalpy of fusion. It was assumed that the cost of the energy provided by the solar furnace, considering amortization, development, and operation, is 0.40 €/kWh. Thus, the cost of melting the fayalite slag in the solar furnace would be 160 €/t slag. It is possible to see that the levelized cost of energy of concentrated solar power plants fell by 47% between 2010 and 2019 (from 0.346 €/kWh to 0.182 €/kWh). The capital cost for concentrated solar power was 1.2–1.8 k€/kW (50–1000 kW) according to Flamant et al., 1999 [63]. On the other hand, the benefit that would be obtained from the recovery of 2.0% Cu in the slags at the current price of the slag (around 9000 €/t Cu in the London Metals Exchange Market) would be 190 €/t slag of fayalite treated with concentrated solar power. If it is considered

that 50% of the magnetite could be recovered per ton of fayalite slag being processed, the benefit would be 300 €/t slag.

The presented results show that some of the fayalite was transformed into magnetite, and some of the initial copper oxides and sulfides were transformed into metallic copper. Considering the separation of the phases (magnetite, metallic copper, and clean slag), it would be possible to take advantage of the properties of the different phases: physical (metallic copper has a density close to 9 g/cm³, magnetite has a density of around 6 g/cm³, and the slag has a density of around 3–4 g/cm³), electrical (electrical properties of the copper can be considered to separate it from the slag), and magnetic (magnetite can be separated using magnetic methods). Grinding operations should be considered before the separation. If the size of the copper nodules is considered, the treated slag should be fine-grinded to less than 10 µm, although this size would require an energy-consuming process, so conditions to have larger copper nodules should be further studied.

The recycling and reutilization of materials has become an important subject for modern societies to comply with environmental regulations and, therefore, improve people's quality of life, for instance in the case of plastics [64] or other metallurgical by-products. In addition, recycling and reutilization of materials increases the efficiency of the industrial processes and, thus, the economic profitability of the industrial sector. In this context, new uses are being given to industrial wastes [65–68] and new potential processes are being considered, such as solar energy [69]. In this manuscript, we proposed the utilization of concentrated solar power (CSP) in the treatment of copper slag to recover/concentrate copper and iron from these slags. The recovery of these valuable phases would reduce the volume of wastes generated in copper metallurgy and, therefore, the environmental impact of metals industries.

5. Conclusions

Slags from copper metallurgy are a residue/by-product of great interest due to the high quantity of iron (>40 wt. %), but also due to the copper content (1–2 wt. %). Conventional recovery of copper from copper slags involves electric furnaces and additions of carbon and pyrite, being energetically intensive and giving as a result slag with 1–2 wt. % in optimal conditions. The copper in the slag is usually matte (Cu₂S·FeS) or an oxide associated with the other oxides of the slag. The problem of electric furnaces is the energy consumption. Concentrated solar power (CSP) could be an alternative in the treatment of copper slags due to the great potential in high-temperature processes, such as those involved in most metallurgical processes. The utilization of CSP in the treatment of copper slags was proposed in this manuscript.

Thermal decomposition of fayalite is thermodynamically favorable at the temperatures and conditions involved in the process. The presence of an oxidizing environment leads to the decomposition of the fayalite but the reduction of copper oxide to metallic copper requires reductant conditions. Both processes compete with each other, as different conditions are required, so searching for a situation where the maximum quantities of both phases are recovered should be considered. The results indicate that fayalite was partially decomposed during the experiments into magnetite and silica because the slag became magnetic after the treatment and the magnetite content significantly increased. However, the fayalite decomposition was not complete since it was still detected in the treated samples. Moreover, copper nodules (65–85 wt. % Cu) were identified in the treated samples, while the initial slag, analyzed by X-ray diffraction, X-ray fluorescence, and SEM-EDX, did not show the presence of metallic copper.

Finally, samples of treated slag were crushed and grinded down to 40 µm with the aim of separating the iron and copper. Two fractions were obtained by magnetic separation: a magnetic fraction (85%), mainly comprised of iron as magnetite; and a non-magnetic fraction (15%) that was a copper concentrate with 5–10 wt. % Cu. Considering the experimental results, 7.5–18 kg Cu/t slag might be recovered from the slag.

A preliminary economic analysis, considering the current copper price, indicates that only the recovery of copper could represent a significant economic benefit (>30 €/t slag). Therefore, CSP might be a potential candidate for the treatment of copper slags to recover copper and iron, although further research is still required to think about the scalation of the process up to the industrial level.

Author Contributions: D.F.-G. and L.F.V. designed the experiments; D.F.-G., Í.R.-B., and C.G.-G. performed the experiments; D.F.-G. and J.P. analyzed the results; D.F.-G. and L.F.V. interpreted the results; D.F.-G. and C.G.-R. wrote the manuscript. All authors have read and agreed to the published version of the manuscript.

Funding: Financial support from the Access to Research Infrastructures activity in the 7th Framework Program of the EU (SFERA 2 Grant Agreement No. 312643) is gratefully acknowledged and the use of the facilities and researchers/technology experts. This research was also supported by a Juan de la Cierva Formación grant from the Spanish Ministry of Science and Innovation (MCINN) to Daniel Fernández-González (FJC2019-041139-I).

Acknowledgments: The authors want to acknowledge the X-ray Diffraction Laboratory at the Faculty of Materials Science and Ceramics of AGH University of Science and Technology (Head of the laboratory, Bartosz Handke) in Krakow for X-ray diffraction and X-ray fluorescence measurements.

Conflicts of Interest: The authors declare no conflict of interest.

References

1. Sancho, J.P.; Verdeja, L.F.; Ballester, A. *Metalurgia Extractiva. Volumen II. Procesos de Obtención*, 1st ed.; Síntesis: Madrid, Spain, 2000.
2. Fan, Y.; Shibata, E.; Iizuka, A.; Nakamura, T. Crystallization behaviors of copper smelter slag studied using time-temperature-transformation diagram. *Mater. Trans.* **2014**, *55*, 958–963. [[CrossRef](#)]
3. Davenport, W.G.; King, M.; Schlesinger, M.; Biswas, A.K. *Extractive Metallurgy of Copper*, 4th ed.; Pergamon-Elsevier Science Ltd.: Oxford, UK, 2002.
4. Nazer, A.; Pavez, O.; Rojas, F.; Aguilar, C. Una revisión de los usos de las escorias de cobre. In Proceedings of the IBEROMET XI. X CONAMET/SAM, Viña del Mar, Chile, 2–5 November 2010.
5. Coursol, P.; Cardona, N.; Mackey, P.; Bell, S.; Davis, B. Minimization of copper losses in copper smelting slag during electric furnace treatment. *JOM* **2012**, *64*, 1305–1313. [[CrossRef](#)]
6. Cardona, N.; Coursol, P.; Vargas, J.; Parra, R. Physical chemistry of copper smelting slags and copper losses at the Paipote smelter. Part 1-Thermodynamic modelling. *Can. Metall. Quart.* **2011**, *50*, 318–329. [[CrossRef](#)]
7. Cardona, N.; Coursol, P.; Vargas, J.; Parra, R. Physical chemistry of copper smelting slags and copper losses at the Paipote smelter. Part 2-Characterization of industrial slags. *Can. Metall. Quart.* **2011**, *50*, 330–340. [[CrossRef](#)]
8. Madheswaran, C.K.; Ambily, P.S.; Dattatreya, J.K.; Rajamane, N.P. Studies on use of copper slag as replacement material for river sand in building constructions. *J. Inst. Eng. Ser. A* **2014**, *95*, 169–177. [[CrossRef](#)]
9. Nazer, A.; Pavez, O.; Rojas, F. Use of copper slag in cement mortar. *REM Rev. Esc. Minas* **2012**, *65*, 87–91. [[CrossRef](#)]
10. Shi, C.; Meyer, C.; Behnood, A. Utilization of copper slag in cement and concrete. *Resour. Conserv. Recy.* **2008**, *52*, 1115–1120. [[CrossRef](#)]
11. Potysz, A.; Van Hullebusch, E.D.; Kierczak, J.; Grybos, M.; Lens, P.N.L.; Guibaud, G. Copper metallurgy slags- Current knowledge and fate: A review. *Crit. Rev. Env. Sci. Tec.* **2015**, *45*, 2424–2488. [[CrossRef](#)]
12. Palacios, J.; Sánchez, M. Wastes as resources: Update on recovery of valuable metals from copper slags. *Miner. Process. Extr. Metall.* **2011**, *120*, 218–223. [[CrossRef](#)]
13. Cendoya, P. Efecto en la resistencia de las escorias de fundición de cobre como agregado fino en el comportamiento resistente del hormigón. *Ingeniare Rev. Chil. Ing.* **2009**, *17*, 85–94. [[CrossRef](#)]
14. Murari, K.; Siddique, R.; Jain, K.K. Use of waste copper slag, a sustainable material. *J. Mater. Cycles. Waste Manag.* **2015**, *17*, 13–26. [[CrossRef](#)]
15. Kambham, K.; Sangameswaran, S.; Datar, S.R.; Kura, B. Copper slag: Optimization of productivity and consumption for cleaner production in dry abrasive blasting. *J. Clean Prod.* **2007**, *15*, 465–473. [[CrossRef](#)]
16. Jiménez-Padilla, B. *Armado de Tuberías. FMEC0108*, 1st ed.; IC Editorial: Antequera, Spain, 2014.
17. Biswas, S.; Satapathy, A. Use of copper slag in glass-epoxy composites for improved wear resistance. *Waste Manag. Res.* **2010**, *28*, 615–625. [[CrossRef](#)]
18. Pundhir, N.K.S.; Kamaraj, C.; Nanda, P.K. Use of copper slag as construction material in bituminous pavements. *J. Sci. Ind. Res. India.* **2005**, *64*, 997–1002.
19. Busolic, D.; Parada, F.; Parra, R.; Sánchez, M.; Palacios, J.; Hino, M. Recovery of iron from copper flash smelting slags. *Miner. Process. Extr. Metall.* **2011**, *120*, 32–36. [[CrossRef](#)]

20. Guo, Z.; Zhu, D.; Pan, J.; Wu, T.; Zhang, F. Improving beneficiation of copper and iron from copper slag by modifying the molten copper slag. *Metals* **2016**, *6*, 86. [[CrossRef](#)]
21. Xian-Lin, Z.; De-Qing, Z.; Jian, P.; Teng-Jiao, W. Utilization of waste copper slag to produce directly reduced iron for weathering resistant steel. *ISIJ Int.* **2015**, *55*, 1347–1352. [[CrossRef](#)]
22. Heo, J.H.; Chung, Y.; Park, J.H. Recovery of iron and removal of hazardous elements from waste copper slag via a novel aluminothermic smelting reduction (ASR) process. *J. Clean. Prod.* **2016**, *137*, 777–787. [[CrossRef](#)]
23. Siwiec, G.; Sozanska, M.; Blacha, L.; Smalcerz, A. Behaviour of iron during reduction of slag obtained from copper flash smelting. *Metabk* **2015**, *54*, 113–115.
24. Sarfo, P.; Wyss, G.; Ma, G.; Das, A.; Young, C. Carbothermal reduction of copper smelter slag for recycling into pig iron and glass. *Miner. Eng.* **2017**, *107*, 8–19. [[CrossRef](#)]
25. Liao, Y.; Zhou, J.; Huang, F. Separating and recycling of Fe, Cu, Zn from dumped copper slag by microwave irradiation assisted carbothermic method. *J. Residuals Sci. Technool.* **2016**, *13*, S155–S160. [[CrossRef](#)]
26. Li, K.; Ping, S.; Wang, H.; Ni, W. Recovery of iron from copper slag by deep reduction and magnetic beneficiation. *Int. J. Min. Met. Mater.* **2013**, *20*, 1035–1041. [[CrossRef](#)]
27. Fernández-González, D.; Ruiz-Bustanza, I.; González-Gasca, C.; Piñuela-Noval, J.; Mochón-Castaños, J.; Sancho-Gorostiaga, J.; Verdeja, L.F. Concentrated solar energy applications in materials science and metallurgy. *Sol. Energy* **2018**, *170*, 520–540. [[CrossRef](#)]
28. Murray, J.P.; Flamant, G.; Roos, C.J. Silicon and solar-grade silicon production by solar dissociation of Si_3N_4 . *Sol. Energy* **2006**, *80*, 1349–1354. [[CrossRef](#)]
29. Loutzenhiser, P.G.; Tuerk, O.; Steinfeld, A. Production of Si by vacuum carbothermal reduction of SiO_2 using concentrated solar energy. *JOM* **2010**, *62*, 49–54. [[CrossRef](#)]
30. Murray, J.P. Aluminum production using high-temperature solar process heat. *Sol. Energy* **1999**, *66*, 133–142. [[CrossRef](#)]
31. Murray, J.P. Aluminum-silicon carbothermal reduction using high-temperature solar process heat. In Proceedings of the 128th TMS Annual Meeting, San Diego, CA, USA, 28 February–4 March 1999.
32. Murray, J.P. Solar production of aluminum by direct reduction: Preliminary results for two processes. *J. Sol. Energy Eng.* **2001**, *123*, 125–132. [[CrossRef](#)]
33. Lytvynenko, Y.M. Obtaining aluminum by the electrolysis with the solar radiation using. *Appl. Sol. Energy* **2013**, *49*, 4–6. [[CrossRef](#)]
34. Epstein, M.; Olalde, G.; Santén, S.; Steinfeld, A.; Wieckert, C. Towards the industrial solar carbothermal production of zinc. *J. Sol. Energ.* **2008**, *130*, 014501–014504. [[CrossRef](#)]
35. Fletcher, E.A.; Noring, J.E. High temperature solar electrothermal processing—Zinc from zinc oxide. *Energy* **1983**, *8*, 247–254. [[CrossRef](#)]
36. Fletcher, E.A.; Macdonald, F.J.; Kunnerth, D. High temperature solar electrothermal processing—II. Zinc from zinc oxide. *Energy* **1985**, *10*, 1255–1272. [[CrossRef](#)]
37. Palumbo, R.D.; Fletcher, E.A. High temperature solar electrothermal processing—III. Zinc from zinc oxide at 1200–1675K using a non-consumable anode. *Energy* **1988**, *13*, 319–332. [[CrossRef](#)]
38. Osinga, T.; Frommherz, U.; Steinfeld, A.; Wieckert, C. Experimental investigation of the solar carbothermic reduction of ZnO using a two-cavity solar reactor. *J. Sol. Energ.* **2004**, *126*, 633–637. [[CrossRef](#)]
39. Epstein, M.; Ehrensberger, K.; Yogev, A. Ferro-reduction of ZnO using concentrated solar energy. *Energy* **2004**, *29*, 745–756. [[CrossRef](#)]
40. Steinfeld, A.; Brack, M.; Meier, A.; Weidenkaff, A.; Wuillemin, D. A solar chemical reactor for co-production of zinc and synthesis gas. *Energy* **1998**, *23*, 803–814. [[CrossRef](#)]
41. Wieckert, C.; Palumbo, R.; Frommherz, U. A two-cavity reactor for solar chemical processes: Heat transfer model and application to carbothermic reduction of ZnO. *Energy* **2004**, *29*, 771–787. [[CrossRef](#)]
42. Wieckert, C.; Frommherz, U.; Kräupl, S.; Guillot, E.; Olalde, G.; Epstein, M.; Santén, S.; Osinga, T.; Steinfeld, A. A 300 kW solar chemical pilot plant for the carbothermic production of zinc. *J. Sol. Energy* **2006**, *129*, 190–196. [[CrossRef](#)]
43. Schunk, L.O.; Lipinski, W.; Steinfeld, A. Heat transfer model of a solar receiver-reactor for the thermal dissociation of ZnO—Experimental validation at 10 kW and scale-up to 1 MW. *Chem. Eng. J.* **2009**, *150*, 502–508. [[CrossRef](#)]
44. Villasmil, W.; Brkic, M.; Wuillemin, D.; Meier, A.; Steinfeld, A. Pilot scale demonstration of a 100-kWth solar thermochemical plant for the thermal dissociation of ZnO. *J. Sol. Energy* **2013**, *136*, 011016–0111027. [[CrossRef](#)]
45. Koepft, E.; Villasmil, W.; Meier, A. Pilot-scale solar reactor operation and characterization for fuel production via the Zn/ZnO thermochemical cycle. *Appl. Energy* **2016**, *165*, 1004–1023. [[CrossRef](#)]
46. Ruiz-Bustanza, I.; Cañadas, I.; Rodríguez, J.; Mochón, J.; Verdeja, L.F.; García-Carcedo, F.; Vázquez, A. Magnetite production from steel wastes with concentrated solar energy. *Steel Res. Int.* **2013**, *84*, 207–217. [[CrossRef](#)]
47. Sibieude, F.; Ducarroir, M.; Tofighi, A.; Ambriz, J. High temperature experiments with a solar furnace: The decomposition of Fe_3O_4 , Mn_3O_4 , CdO . *Int. J. Hydrogen Energy* **1982**, *7*, 79–88. [[CrossRef](#)]
48. Steinfeld, A.; Fletcher, E.A. Theoretical and experimental investigation of the carbothermic reduction of Fe_2O_3 using solar energy. *Energy* **1991**, *16*, 1011–1019. [[CrossRef](#)]

49. Steinfeld, A.; Kuhn, P.; Karni, J. High-temperature solar thermochemistry: Production of iron and synthesis gas by Fe_3O_4 -reduction with methane. *Energy* **1993**, *18*, 239–249. [[CrossRef](#)]
50. Fernández-González, D.; Prazuch, J.; Ruiz-Bustinza, I.; González-Gasca, C.; Piñuela-Noval, J.; Verdeja, L.F. Solar synthesis of calcium aluminates. *Sol. Energy* **2018**, *171*, 658–666. [[CrossRef](#)]
51. Mochón, J.; Ruiz-Bustinza, I.; Vázquez, A.; Fernández, D.; Ayala, J.M.; Barbés, M.F.; Verdeja, L.F. Transformations in the iron-manganese-oxygen-carbon system resulted from treatment of solar energy with high concentration. *Steel Res. Int.* **2014**, *85*, 1469–1476. [[CrossRef](#)]
52. Fernández-González, D.; Prazuch, J.; Ruiz-Bustinza, I.; González-Gasca, C.; Piñuela-Noval, J.; Verdeja, L.F. Iron Metallurgy via Concentrated Solar Energy. *Metals-Basel* **2018**, *8*, 873. [[CrossRef](#)]
53. Fernández-González, D.; Prazuch, J.; Ruiz-Bustinza, I.; González-Gasca, C.; Piñuela-Noval, J.; Verdeja, L.F. The treatment of Basic Oxygen Furnace (BOF) slag with concentrated solar energy. *Sol. Energy* **2019**, *180*, 372–382. [[CrossRef](#)]
54. Fernández-González, D.; Prazuch, J.; Ruiz-Bustinza, I.; González-Gasca, C.; Piñuela-Noval, J.; Verdeja, L.F. Transformations in the Mn-O-Si system using concentrated solar energy. *Sol. Energy* **2019**, *184*, 148–152. [[CrossRef](#)]
55. Fernández-González, D.; Prazuch, J.; Ruiz-Bustinza, I.; González-Gasca, C.; Piñuela-Noval, J.; Verdeja, L.F. Transformations in the Si-O-Ca system: Silicon-calcium via solar energy. *Sol. Energy* **2019**, *181*, 414–423. [[CrossRef](#)]
56. Fernández-González, D.; Prazuch, J.; Ruiz-Bustinza, I.; González-Gasca, C.; Gómez-Rodríguez, C.; Verdeja, L.F. Treatment of copper slag with concentrated solar energy. In *Proceedings of the Environmental Safety-Non-Energy and Raw Materials, I International Conference on Engineering Materials, Safety, Environment and Technology, Zielona Gora, Poland, 3–4 June 2020*; Gabryelewicz, I., Wedrychowicz, M., Eds.; University of Zielona Gora: Zielona Gora, Poland, 2021; pp. 39–59.
57. Winkel, H.E. Thermal Decomposition of Copper Sulfides under Concentrated Irradiation. Ph.D. Thesis, Swiss Federal Institute of Technology Zurich, Zurich, Switzerland, 2006.
58. Alcock, C.B. *Principles of Pyrometallurgy*; Academic Press: London, UK, 1976; pp. 15–16.
59. Ballester, A.; Verdeja, L.F.; Sancho, J.P. *Metalurgia Extractiva. Volumen I. Fundamentos*, 1st ed.; Síntesis: Madrid, Spain, 2000.
60. Richardson, F.D.; Jeffers, J.H.E. The Ellingham diagram for metal oxides. In *Introduction to Metallurgical Thermodynamics*; Hemisphere Publishing Corporation: San Francisco, CA, USA, 1981.
61. Verdeja, L.F.; Sancho, J.P.; Ballester, A. *Refractory and Ceramic Materials*, 1st ed.; Síntesis: Madrid, Spain, 2014.
62. Pero-Sanz, J.A.; Quintana, M.J.; Verdeja, L.F. *Solidification and Solid-state Transformations of Metals and Alloys*, 1st ed.; Elsevier: Boston, MA, USA, 2017.
63. Flamant, G.; Ferriere, A.; Laplace, D.; Monty, D. Solar processing of materials: Opportunities and new frontiers. *Sol. Energy* **1999**, *66*, 117–132. [[CrossRef](#)]
64. Alvarez, M.A. Environmental Impact of Plastics. *J. Mater. Ed.* **2018**, *40*, 119–124.
65. Dobiszewska, M. Waste Materials Used in Making Mortar and Concrete. *J. Mater. Ed.* **2017**, *39*, 133–156.
66. Fernández-González, D.; Sancho-Gorostiaga, J.; Piñuela-Noval, J.; Verdeja, L.F. Anodic Lodes and Scrapings as a Source of Electrolytic Manganese. *Metals* **2018**, *8*, 162. [[CrossRef](#)]
67. Ordiales, M.; Iglesias, J.; Fernández-González, D.; Sancho-Gorostiaga, J.; Fuentes, A.; Verdeja, L.F. Cold agglomeration of Ultrafine Oxidized Dust (UOD) from ferromanganese and silicomanganese industrial process. *Metals* **2016**, *6*, 203. [[CrossRef](#)]
68. Fernández-González, D.; Piñuela-Noval, J.; Verdeja, L.F. Silicomanganese and ferromanganese slags treated with concentrated solar energy. *Proceedings* **2018**, *2*, 1450. [[CrossRef](#)]
69. Fernández-González, D. Aplicaciones de la Energía Solar Concentrada en Metalurgia y Ciencia de los Materiales. Ph.D. Thesis, Department of Materials Science and Metallurgical Engineering, University of Oviedo, Oviedo/Uviéu, Asturias, Spain, September 2019.